A Medium Frequency Transformer-Based Wind Energy Conversion System Used for Current Source Converter Based Offshore Wind Farm

Qiang Wei, Bin Wu, *Fellow, IEEE*, Dewei (David) Xu, *Member, IEEE*, and Navid R. Zargari, *Fellow, IEEE*

***Abstract*—Offshore wind farms with series-interconnected structures are promising configurations because bulky and costly offshore substations can be eliminated. In this work, a medium-frequency transformer (MFT)-based wind energy conversion system is proposed for such wind farms based on current source converters. The presented configuration consists of a medium-voltage permanent magnet synchronous generator that is connected to a low-cost passive rectifier, an MFT-based cascaded converter, and an onshore current source inverter. Apart from fulfilling traditional control objectives (maximum power point tracking, dc-link current control, and reactive power regulation), this work endeavors to ensure evenly distributed power and voltage sharing among the constituent modules given the cascaded structure of the MFT-based converter. In addition, this paper thoroughly discusses the characteristic of decoupling between the voltage/power balancing of the modular converter and the other control objectives. Finally, both simulation and experimental results are provided to reflect the performance of the proposed system.**

***Index Terms*—Current source converter, medium-voltage, permanent magnet synchronous generator, offshore, wind energy conversion system, medium-frequency transformer, cascaded DC-DC converter.**

I. Introduction

AMONG all available renewable energy sources, wind energy (onshore and offshore) has increasingly become a mainstream [1]. Unlike onshore applications, installed offshore wind power capacity accounted for only 2% of the total capacity as of 2012 [2]. Nonetheless, an increasing trend is forecasted because of [3] (a) offshore wind resources are considerable. (b) Offshore wind speed is often significantly higher and steadier than that on land. (c) The environmental effect (audible noise and visual effect) is the minimized in offshore applications.

Qiang Wei, Bin Wu, and David Xu are with the Department of Electrical and Computer Engineering, Ryerson University, 350 Victoria St, Toronto, ON, M5B 2K3, Canada (e-mail: qiang.wei@ryerson.ca; bwu@ee.ryerson.ca; dxu@ryerson.ca).

Navid Reza Zargari is with the Medium Voltage R&D Department, Rockwell Automation Canada, Cambridge, ON N1R5X1, Canada (e-mail: nrzargari@ra.rockwell.com).

On the basis of the connection methods of wind turbines in offshore wind farms and the characteristics of the power to be delivered, the wind energy conversion system (WECS) proposed in literature and implemented practically can be classified into four types [4]–[7], [36]: parallel ac connection and high voltage alternating current (HVAC) transmission systems, parallel ac connection and high voltage direct current (HVDC) transmission systems, parallel dc connection and HVDC transmission systems, and series dc connection and HVDC transmission systems. The HVAC system is suitable for application where the transmission distance is lower than 50 km, while HVDC system dominates the market when the transmission distance is longer than 50 km. All these configurations except the fourth one (series dc connection and HVDC transmission system) need offshore substation which is very bulky and costly. Aside from considering reliability and efficiency as main requisites for all onshore conversion systems, the footprints and weights of the components are particularly important for offshore infrastructure. The total weight of the system that is dominated by the offshore substation significantly affects the cost and complexity of the offshore wind farm [25]. Therefore, the fourth one (series dc connection and HVDC transmission system) is increasingly emphasized in research because it can save significantly cost given that the bulky and costly offshore substation can be eliminated [8].

The electric generators used to convert mechanical energy into electrical energy have been well developed. They are divided in two main groups: induction generators (squirrel-cage, doubly-fed induction generator) and synchronous generators (permanent-magnet, wound-rotor synchronous generator). Among these generators, PMSG is gaining increased attention in the research given its low maintenance cost and negligible rotor loss [3]. Moreover, medium-voltage (MV) PMSG-based WECS with voltage levels that range between 3–4 kV is considered the most suitable and economical approach when a power rating exceeds 3 MW [8].

MV-based power converters, which are crucial components in WECS, can be classified into voltage source converters (VSCs) and current source converters (CSCs). On the one hand, VSC-based WECS dominates offshore wind farm applications.

A two-level VSC in which switching devices are connected in series has been proposed for MV-based WECS [9], and the back-to-back neutral point clamped (NPC)-based WECS is widely studied in previous works [10]–[11]. An active NPC (ANPC)-based WECS was proposed to solve the uneven power loss problem associated with NPC [12]. A four-level diode clamped converter can be used to achieve MV operation levels [13], as well as the multi-level ANPC [14] and matrix converter-based WECS [15]. The power flow in WECS is unidirectional; therefore, low-cost passive converters (diode rectifiers) can be employed at the generator side instead of the aforementioned pulse width modulated (PWM) active converters [16]. On the other hand, CSCs features natural advantages with simple structure, grid-friendly waveforms, controllable power factor, and reliable grid short-circuit protection. In addition, these converters have successfully been used in high-power MV-based industrial drives and are considered to be highly promising converters for MV-based WECS applications [17].

Therefore, the key words of the present work can be highlighted with: (a) CSC-based offshore wind farm; (b) series dc connection and HVDC transmission system; and (c) MV PMSG-based WECS.

Unfortunately, the CSC-based WECS has not been studied extensively in literature. The thyristor-based current source line commutated converter (LCC), which is a proven and well-established technology in HVDC transmission system, has been investigated for WECS application. Ref. [18], [19] focus on techniques for reactive power control and harmonics compensation, while [20] discusses an LCC-based wind farm with series-interconnected structures. However, an LCC-based WECS has the following disadvantages [21]: the need for large passive filters to reduce low-order harmonics, a large footprint, a low dynamic performance, dependent active and reactive power control, and susceptibility to ac network disturbance. A parallel-connected wind farm structure was established in [22] wherein all wind turbine modules are connected in parallel; only one onshore current source inverter (CSI) delivers the total power of the offshore wind farm to the grid. The most significant challenges faced by this configuration are the losses of the transmission cables and the power rating of the onshore CSI that needs to withstand the full power of the wind farm. A back-to-back PWM CSC-based system was proposed to interface a single wind turbine to the grid [23]; on this basis, a series-interconnected structure was proposed for an offshore wind farm where cascaded PWM CSCs are installed on the generator and grid sides [24]. Bulky and costly offshore substations can be eliminated in this configuration; however, a high-power, low-frequency transformer is required for generator insulation because the wind generator that is farthest from the grounding point must be capable of withstanding the full transmission voltage of the offshore wind farm. These bulky transformers increase the burden on offshore construction because of the limited space either in the nacelle or in the tower of the wind turbine [25].

In the present work, a medium frequency transformer (MFT)-based WECS is proposed for series-connected CSC-based offshore wind farms (Fig. 1). The configuration consists of an MV PMSG that is connected to a low-cost three-phase diode rectifier, a modular MFT-based converter, and an onshore CSI connected to the grid through a multi-winding transformer. The present paper mainly focuses on two of the major issues in an offshore wind farm. One is to eliminate the bulky and costly offshore substation, and the other is to eliminate the bulky and heavy low-frequency transformer which is normally installed in the nacelle or inside the tower of the wind turbine [24]. The first issue is solved by using the series-connected wind farm structure, and the second issue is solved by the modular MFT-based converter. There are a number of features associated with the proposed wind farm system, including (a) significant cost reduction due to the elimination of offshore substations; (b) light weight and high power density due to the adaption of an modular MFT-based converter, which facilitates the wind turbine installation and foundation construction; (c) high reliability and flexibility due to the use of modular converters; and (d) all the advantages of the proven MV CSC technology.

Apart from meeting the traditional control objectives of a WECS (maximum power point tracking (MPPT), dc-link current, and reactive power regulation), the current research endeavors to ensure evenly distributed power and voltage sharing among the constituent modules. With the special focus on converter control, the remainder of this paper is organized as follows: the proposed configuration is presented in Section II. The analysis of the modular converter is described comprehensively in Section III. The control scheme for the proposed WECS is thoroughly discussed in Section IV. The simulation and experimental verification process are presented in Section V. Finally, this work is concluded in Section VI.

II. Configuration of The Proposed WECS

Fig. 1 shows the overall structure of the CSC-based offshore wind farm. N numbers of the proposed MV PMSG-based WECSs are connected in series with one common dc-link inductor L_{dc}. The onshore CSIs are connected to the grid through multi-winding transformers. Fig. 2 depicts the topology of the proposed MFT-based WECS; the configuration consists of an MV PMSG, a three-phase diode rectifier, a modular MFT-based converter, and a CSI [17] that is connected to the grid through a transformer. C_f is the output capacitor and L_g represents the grid-side inductance. Fig. 3 illustrates the detailed topology for the modular MFT-based converter, in which N numbers of voltage-fed, current-output converters (without an output capacitor filter) are connected in series, then directly connected to the dc-link inductor L_{dc}. C_N (N = 1, 2 …, N) is input capacitor of each module in the cascaded converter.

As a front-end converter, the passive rectifier displays the advantages of reliability, low-cost, being small and light, and having a simpler generator-side control than a PWM converter dose. On the other hand, the passive rectifier leads to a relatively high torque ripple in the generator. However, various methods have been proposed in literature to solve this problem [26]. Furthermore, the synchronous inductance of a PMSG is usually above 0.4 per unit (pu) for high-power, low-speed wind

applications [23], which further helps to mitigate the torque ripple [17].

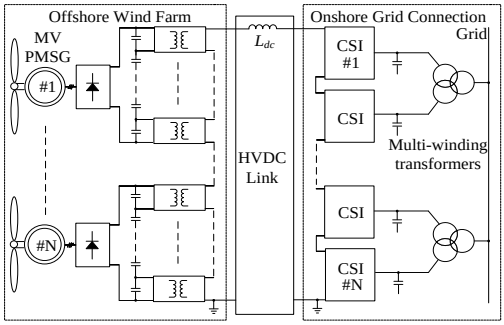

Fig. 1. Proposed configuration of CSC-based offshore wind farm.

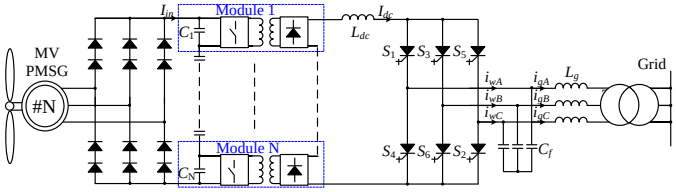

Fig. 2. Proposed MFT-based WECS.

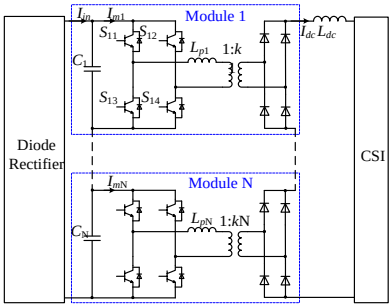

Fig. 3. Modular DC-DC converter.

In a series-connected wind farm, generator insulation should be carefully considered. The wind generator that is farthest from the grounding point must be capable of withstanding full transmission voltage. MFTs are employed to alleviate this problem. Compared with other methods in literature [37], a transformer-based solution seems more reasonable when considered in practice [33], while compared with method in [33] where a high-power (same power with each PMSG-based WECS) low-frequency three-phase transformer is employed, the proposed modular MFTs-based solution is advantages in terms of higher power density, small footprint and weight (which is much more important for offshore application). In addition, by the proposed MFT-based converter, only secondary-side components of MFTs (diodes rectifier) are needed for high voltage insulation, while both offshore converters and capacitors are needed in [33]. As shown in Fig. 1, all the components are similarly rated, but the insulation levels are not uniform. The insulation requirement is reduced when the wind turbine unit is located near the ground point.

A coordinated control scheme was proposed for a series-connected CSC-based offshore wind farm in a previous study [24]. By contrast, the current work focuses on the control scheme of the single MV PMSG-based WECS (Fig. 2).

III. Analysis of The Modular Converter

The modular converter (Fig. 3) plays crucial roles in the proposed WECS. First, it is beneficial for achieving both MPPT and grid-side control [27]. Second, MFT is employed because of the generator insulation issue which has been discussed in the previous section, thus not repeated here. Instead of using bulky low-frequency transformers [24], MFTs are employed given their advantages of high power density and easy offshore construction. Furthermore, a modular design is implemented based on a number of cells that are connected in series at the input and output. In contrast to a single MFT, such design helps reduce the burden of implementation as one transformer accounts for only one part of a megawatt-level power. The modular design of the converter also benefits from the choice of low-cost, low-voltage switching devices instead of high-voltage ones. Increasing operating frequency results in a large reduction in size and weight of the transformer. However, in the application MV Megawatts-level WECS, several challenges should be considered [38]: (a) Losses and thermal design. A significant challenge will be introduced to thermal and cooling system design due to the combination of small size and high losses as increasing operation frequency; (b) challenge coming from the insulation design of high-power MFT. In applications of series-connected wind farm, the maximum potential the transformer must withstand is the full transmission level. This is a significant issue as its considerable effect on the size of the transformer. Therefore, in practice, an optimum design should be a trade-off between operation frequency and size to achieve a best overall performance which is not addressed in the present work. A 4000 V PMSG-based WECS is presented to illustrate the design process.

A. Determination of the number of cells

The minimum required number of cells for the proposed configuration depends on: (a) input dc voltage, (b) the voltage rating of the selected insulated-gate bipolar transistor (IGBT), and (c) the chosen cell voltage. The rated input dc voltage is approximately 5000 V for a 4000 V PMSG-based system. 1700 V IGBT is selected because it is the most suitable switching device in terms of cost, voltage utilization, and failure in time rate for MV applications [28]. Given a cell voltage of 1000 V [17], five cells (without redundancy) must be connected in series at both the input and the output. A converter with six cells can also be chosen for redundancy (N+1); nonetheless, this work considers a modular converter with five cells.

B. MFT

The topology of each module that is employed in the MFT-based converter (Fig. 3) is a voltage-fed, current-output, full-bridge converter with a common inductor (L_{dc}) filter. In this study, the MFT plays two roles: First, this transformer can help realize zero-voltage switching for the primary switches through leakage inductance L_{pN} (N = 1, 2 …, 5) without requiring additional components [29]. Second, MFT performs an isolation function. As mentioned in the previous section, the MFT must withstand a full transmission voltage at most; hence the issue of MFT insulation must be considered in practical design and manufacture [30].

C. Input capacitor voltages sharing in the modular converter

The constituent modules of the modular converter (Fig. 3) are designed to be identical. Given existing manufacturing techniques, however, the components used may not display exactly same characteristics. For example, the turn ratios of MFTs may be slightly mismatched with 1: $k1 \neq 1$: $k2 \neq \ldots$ 1: $k5$ (Fig. 3). As a result, the operation of the cascaded converter is destabilized if a common duty ratio alone is employed [31]. The module with the lowest turn ratio has highest input capacitor voltage and constitutes the largest proportion of total power. Therefore, input capacitor voltages must be shared among the constituent modules. This aspect is thoroughly discussed in the next section.

D. Operation Principle

One advantage of a modular converter is its control scheme can be simplified that all constituent modules share the same control. It means the drive signals for S_{11}, S_{21} … S_{51} are same (Fig. 3) and so are other switches. Here, we take Module 1 as an example to illustrate the operation principle. The conventional phase-shifted modulation scheme is employed where all the switches operate with fixed 50% duty cycle, while the phase of the second leg is shifted to transfer the power. The steady state waveform is shown in Fig. 4 where the dead time between switches in the same leg is not shown. S_{11}, S_{12}, S_{13}, and S_{14} are the corresponding drive signals; I_{dc} and i_{p1} are dc-link current and transformer primary currents (Fig. 3), respectively; V_{o1} is the output voltage. The corresponding operation states are shown in Fig. 5. Before t_0, switches S_{11} and S_{14} are on, and so are D_{11} and D_{14} (Fig. 5 [a]). The transformer primary/secondary currents i_{p1}/i_{s1} and the output voltage V_{o1} are now kept at 1 pu, and the power is transferred to the load. $t_0 < t < t_1$: At time t_0, S_{14} is turn off, primary current i_{p1} commutates from S_{14} to the parallel diode of S_{12} during the dead time; therefore, S_{12} is turn on with zero voltage switching (ZVS). During this period, currents i_{p1}/i_{s1} are slightly decreasing to less than 1 pu, while the dc-link current I_{dc} is controlled to maintain at 1 pu by the CSI; therefore, D_{12} and D_{13} are turn on (D_{11} and D_{14} are staying on). The output voltage V_{o1} is now staying at 0 pu, and no power is transferred (Fig. 5 [b]). $t_1 < t < t_2$: At time t_1, S_{11} is turn off, and as same as that in the previous period, S_{13} is turn on with ZVS. Currents i_{p1}/i_{s1} is now decreasing sharply with the slope determined by the input voltage and the value of the leakage inductor. During this period, D_{11}, D_{12}, D_{13} and D_{14} are still kept on and no power is transferred (Fig. 5 [c]). $t_2 < t < t_3$: At time t_2, Currents i_{p1}/i_{s1} is decreasing to –1 pu; meanwhile, D_{11} and D_{14} are turn off, while D_{12} and D_{13} are kept on. The output voltage V_{o1} is now staying at 1 pu, and the power is transferred to the load (Fig. 5 [d]). $t_3 < t < t_4$: At time t_3, S_{12} is turn off; S_{14} is turn on with zero voltage switching (ZVS). The operation principle is same as that during $t_0 < t < t_1$. Thus is not repeated here (Fig. 5 [e]). After t_4, same operation cycle repeats as shown in Fig. 4.

IV. Control Scheme of The Proposed WECS

The control scheme is developed in accordance with direct requirements of the WECS itself and the characteristics of the proposed configuration. Overall control targets are identified as: (1) MPPT in the full operation; (2) input capacitor voltage sharing of the modular converter; (3) minimum dc-link current control; and (4) reactive power control. Fig. 6 illustrates the overall control scheme of the proposed WECS, where MPPT and input capacitor voltage balance control are achieved with the generator-side converter while minimum dc-link current and reactive power control are regulated by the grid-side CSI. All the symbols used in the remainder of this paper correspond to those shown in this figure.

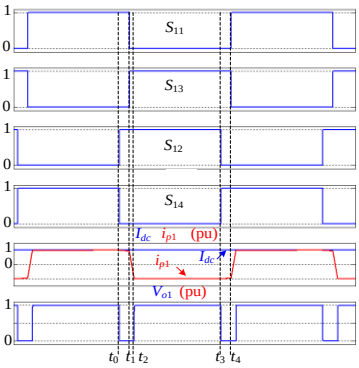

Fig. 4. Steady State waveform of Module 1.

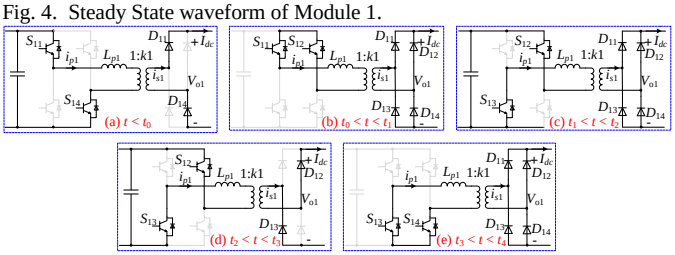

Fig. 5. Operation States of Module 1.

A. Generator-side control

Two objectives are controlled at the generator side: MPPT and capacitor voltage sharing. In a variable-speed WECS, generator speed is adjusted to achieve MPPT. MPPT methods are widely discussed in literature [3], including MPPT with turbine power profiles, optimal tip speed ratios, and optimal torque control. The current study mainly focuses on converter control; therefore, the simple optimal tip speed ratio is applied to achieve MPPT.

If the modular converter is ideal that all the involved components of the five constituent modules are identical, then the captured wind power is evenly distributed among them. The cascaded converter can thus be simplified to one H-bridge converter with a common duty cycle d_{common} and then into a simple Buck converter where the leakage inductance of the transformer is disregarded (Fig. 7). Measured wind speed v_{wind} is used to determine the generator speed reference w_{m_ref} according to the optimal tip ratio (Fig. 6). The regulator output is denoted by torque reference T_{g_ref} of the generator, which is proportional to the corresponding generator current $I_{dc\_generator}$. P and λ are the pole pairs and flux of the PMSG (Fig. 6). The required duty cycle d_{common} for the dc-dc converter is obtained by comparing $I_{dc\_generator}$ and DC-link current I_{dc}. MPPT is achieved upon applying the common duty cycle d_{common} to the dc-dc converter. For example, the amount of captured wind power increases with wind speed; thus, $I_{dc\_generator}$ and duty cycle d_{common} increase as well.

This article has been accepted for publication in a future issue of this journal, but has not been fully edited. Content may change prior to final publication. Citation information: DOI 10.1109/TPEL.2016.2524635, IEEE Transactions on Power Electronics

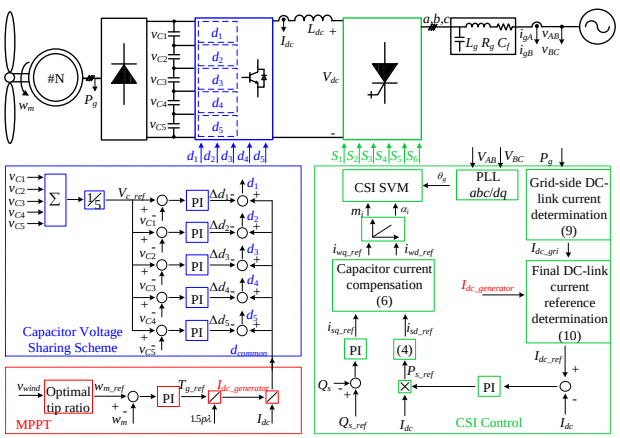

Fig. 6. Overall control scheme of the proposed configuration.

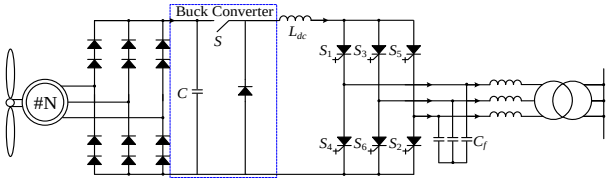

Fig. 7. Ideally simplified configuration of the proposed WECS.

However, the parameters of the five constituent modules cannot be identical in practice due to existing manufacturing techniques. As mentioned in the previous section, the turn ratios of MFTs may be mismatched with 1: $k1 \neq 1$: $k2 \neq \ldots$ 1: $k5$ (Fig. 3). Then the scheme that utilizes only the aforementioned common duty cycle d_{common} destabilized operations with unevenly distributed power among the constituent modules and an imbalance in the input capacitor voltages. Therefore, special attention must be paid to the capacitor voltage balance and power sharing of the cascaded converter.

The dc-link current is controlled by the CSI. Therefore, the equivalent circuit of the MFT-based cascaded dc-dc converter is derived shown in Fig. 8, where input voltage V_{in} is the output voltage of the rectifier. I_{in} is the input current of the MFT-based cascaded dc-dc converter the dc-link current; I_{dc} is represented by a constant current source. In this research, V_{in} and I_{dc} are variable according to different wind speeds and constant at a given speed.

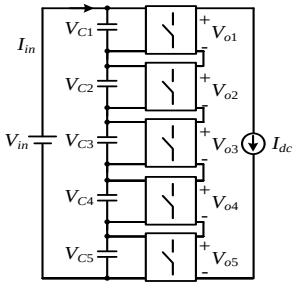

Fig. 8. Equivalent circuit of the MFT-based cascaded DC-DC converter.

The MFT-based converter is connected in series at the input and the output. Such converters shares input and output currents I_{in} and I_{dc}, respectively. Through power conservation, the following is obtained:

$$\begin{cases} P_{in1} = V_{C1} I_{in} = V_{o1} I_{dc} = P_{o1} \\ P_{in2} = V_{C2} I_{in} = V_{o2} I_{dc} = P_{o2} \\ \vdots \\ P_{in5} = V_{C5} I_{in} = V_{o5} I_{dc} = P_{o5} \end{cases} \quad (1)$$

where V_{C1}, V_{C2} ... and V_{C5}, and V_{o1}, V_{o2} ... and V_{o5} are the equilibrium values of the input and output voltages of the constituent modules, respectively. P_{in1}, P_{in2} ... and P_{in5}, and P_{o1}, P_{o2} ... and P_{o5} are the input and output power of each module, respectively. Assuming that the input capacitor voltage is balanced:

$$V_{C1} = V_{C2} = \ldots = V_{C5} = \frac{V_{in}}{5} \quad (2)$$

Then, output voltage is automatically achieved. Furthermore, total power can be distributed evenly among all the modules. Therefore, we need only focus on input capacitor voltage sharing to achieve both input/output voltages and power sharing in the MFT-based cascaded dc-dc converter.

The constituent modules of the dc-dc converter essentially belong to a Buck converter with the following input/output characteristics:

$$\begin{cases} V_{o1} = f(d_1) V_{C1} \\ V_{o2} = f(d_2) V_{C2} \\ \vdots \\ V_{o5} = f(d_5) V_{C5} \end{cases} \quad (3)$$

where d_1, d_2 …, and d_5 are the duty cycles and $f(d_1)$, $f(d_1)$ …, and $f(d_5)$ are the voltage gains of each converter under steady state.

The proposed control scheme of capacitor voltage balancing (Fig. 6) adjusts the duty cycles in (3) to achieve the even distribution of input capacitor voltages. The applied duty cycles d_1, d_2 …, and d_5 are composed of two parts: one is the common duty cycle d_{common} that represents MPPT, and the other represents the individual parts Δd_1, Δd_2 …, and Δd_5 that originate from the regulation of input capacitor voltage balancing. Under the common duty cycle d_{common}, the module with a larger turn ratio tends to draw higher input current than other modules do. This occurrence is impossible under steady state because the series connection at the input mandates that the input currents of the constituent modules should be equal. Hence, the capacitor of the module with a larger turn ratio must discharge more to compensate for the required current; this discharge lower capacitor voltage more in this module than in others. Therefore, input voltage loops (Fig. 6) are established to regulate individual input capacitor voltage by using PI controllers. The regulator output is obtained by adjusting the duty cycles required for voltage balancing. In contrast to the common duty cycle d_{common}, the module with a higher input capacitor voltage has a higher duty cycle with $d_{common} + \Delta d$. In the process, additional power is transferred to the load; thus, more power is discharged from the capacitor. The regulation continues until voltages are balanced.

B. Grid-side control

The major control objectives for the grid-side CSI are dc-link current and reactive power control. Unlike in VSC-based WECS where dc-link voltage is normally controlled at a constant value, the dc-link current in CSC-based WECS is variable according to different levels of captured power to minimize loss [17]. It is determined by both the generator and the grid side to achieve (a) all the control objectives and (b) a minimum WECS loss [34].

As shown in Fig. 6, dc-link current regulation adjusts the captured wind power while reactive power control is implemented to regulate reactive power according to the grid codes. The Grid-voltage phase-locked loop (PLL) is employed to generate a noise-free synchronous angle θ_g and angular frequency ω_g . Given the aligned synchronous frame, the active and reactive power (P_s, Q_s) can be controlled independently by the following:

$$P_s = 1.5 V_{sd} i_{sd} \tag{4}$$

$$Q_s = -1.5 V_{sd} i_{sq} \tag{5}$$

where V_{sd} and V_{sq} and i_{sd} and i_{sq} are the *d*- and *q*-axis components of the grid voltage and injected current.

The reference current of the CSI i_{wd_ref} and i_{wq_ref} can be derived with the following [17], [23]:

$$\begin{cases} i_{wd\_ref} = i_{sd\_ref} + i_{cd} = i_{sd\_ref} - \omega_g C_f V_{cq} \\ i_{wq\_ref} = i_{sq\_ref} + i_{cq} = i_{sq\_ref} + \omega_g C_f V_{cd} \end{cases} \tag{6}$$

where i_{sd_ref} and i_{sq_ref} are the references of the *d*- and *q*-axis components of the injected grid current. i_{cd}, i_{cq} and V_{cd}, V_{cq} are *d*- and *q*-axis components of the capacitor current and the voltage; these variables can be expressed as follows:

$$\begin{cases} V_{cq} = R_g i_{sd} + V_{sd} - \omega_g L_g i_{sq} \\ V_{cq} = R_g i_{sq} + \omega_g L_g i_{sd} \end{cases} \tag{7}$$

where L_g and R_g represent the grid-side line inductance and resistance, respectively.

Without loss consideration of the converter, the captured wind power is equal to the grid-injected power.

$$P_s = P_g \tag{8}$$

With considering the maximum modulation index as m_i = 1 [17], the minimum dc-link current I_{dc_grid} determined by the grid-side CSI can be derived based on (4)–(8):

$$I_{dc\_grid} = \sqrt{\left\{(1-\omega_g^2 L_g C_f)\left(\frac{2}{3}\frac{P_g}{V_{sd}}\right) - \omega_g R_g C_f \left(\frac{2}{3}\frac{Q_{s\_ref}}{V_{sd}}\right)\right\}^2 + \left\{(1-\omega_g^2 L_g C_f)\left(\frac{2}{3}\frac{Q_{s\_ref}}{V_{sd}}\right) + \omega_g C_f V_{sd} + \omega_g R_g C_f \left(\frac{2}{3}\frac{P_g}{V_{sd}}\right)\right\}^2} \tag{9}$$

Therefore, the final minimum dc-link current reference I_{dc_ref}, is expressed as:

$$I_{dc\_ref} = \max\left(I_{dc\_grid}, I_{dc\_generator}\right) \tag{10}$$

where $I_{dc\_generator}$ is the minimum dc-link current determined by the generator-side, as indicated in Fig. 6.

By applying the minimum dc-link current reference, the WECS can therefore achieve the required control objectives and minimized loss.

C. Decoupled characteristics between voltage balance control and other control objectives of the WECS

On the basis of control scheme presented in Fig. 6, we can get:

$$\begin{cases} d_1 = d_{common} - \Delta d_1 \\ d_2 = d_{common} - \Delta d_2 \\ d_3 = d_{common} - \Delta d_3 \\ d_4 = d_{common} - \Delta d_4 \\ d_5 = d_{common} - \Delta d_5 \end{cases} \tag{11}$$

Under steady state, the following equation is valid when same PI controllers are employed.

$$\begin{cases} \Delta d_1 = k\left(\frac{V_{C1}+V_{C2}+V_{C3}+V_{C4}+V_{C5}}{5} - V_{C1}\right) \\ \Delta d_2 = k\left(\frac{V_{C1}+V_{C2}+V_{C3}+V_{C4}+V_{C5}}{5} - V_{C2}\right) \\ \Delta d_3 = k\left(\frac{V_{C1}+V_{C2}+V_{C3}+V_{C4}+V_{C5}}{5} - V_{C3}\right) \\ \Delta d_4 = k\left(\frac{V_{C1}+V_{C2}+V_{C3}+V_{C4}+V_{C5}}{5} - V_{C4}\right) \\ \Delta d_5 = k\left(\frac{V_{C1}+V_{C2}+V_{C3}+V_{C4}+V_{C5}}{5} - V_{C5}\right) \end{cases} \tag{12}$$

where *k* is the gain of the PI controller under steady state. Combining (11) and (12) leads to

$$\frac{d_1+d_2+d_3+d_4+d_5}{5} = d_{common} \tag{13}$$

Equation (13) reveals that voltage balance control and the generator control are decoupled. On the other hand, the relationship between generator-side and grid-side control is not completely decoupled during the full operation range as the final dc-link current reference is the minimum reference between the generator-side and grid-side currents. However, the voltage/power balance control of the MFT-based modular dc-dc converter is decoupled with the grid-side control objectives (dc-link current control, and reactive power control) because of (13).

V. Simulation and Experimental Results

The performance of the proposed configuration has been verified by both Matlab/Simulink simulation and experimental tests. The system parameters used are listed in Table I.

TABLE I
Simulation And Experimental Parameters

Parameters	Simulation		Experiment	
	SI	pu	SI	pu
System Rating				
Nominal Power	1 MW	1.0	1275W	1.0
Grid Voltage	4160 V	1.0	208 V	1.0
Frequency	60 Hz	1.0	60 Hz	1.0
PMSG				
Nominal Power	4000 V		Voltage Source Supply	
synchronous Inductance	0.4 pu			
Stator Resistance	0.01 pu			
Number of Poles	16			
Generators-side converter (MFT-based converter)				
Number of Modules	5		3	
Turn Ratios of Transformers	1 : 1/1 : 1.005 1 : 1.01/1 : 1.015 1 : 1.02		1 : 1/ 1 : 1/ 1 : 1 Tolerance ± 2%	
Input Capacitor (C_N)	200 uF	2.0	1000 uF	2.0
Switching Frequency (f_{sw1})	1200Hz	1.0	1200 Hz	1.0
Grid-side converter (CSI)				
DC-link Inductor (L_{dc})	30 mH	0.65	60 mH	0.65
Grid-side inductor (L_g)	2.55mH	0.055	5 mH	0.055
Grid-side Capacitor (C_f)	153 uF	1.0	80 uF	1.0
Switching Frequency (f_{sw})	540 Hz	1.0	540 Hz	1.0
Modulation Scheme	SVM		SVM	

A. Simulation Results

The wind turbine and the PMSG used in this simulation are provided by Matlab/Simulink. The turbine model receives the wind speed and provides an optimized reference speed to the

control system. The inertia constant of a megawatts-level WECS is normally around a few seconds [23]; in this simulation, the constant is reduced to achieve a faster speed response compared with that in a real system. Five modules are employed in the MFT-based converter; to introduce imbalance into this converter, the turn ratios of the five transformers are purposely set to 1:1 (Module 1), 1:1.005 (Module 2), and 1:1.01 (Module 3), 1:1.015 (Module 4), and 1:1.02 (Module 5). In the following simulation, three typical operations are conducted: (a) with/without voltage balance control, (b) under stepped change in wind speed, and (c) under reactive power control.

Fig. 9 illustrates the simulated performance under conditions of unity power factor (UPF) and with/without voltage balance control scheme (Fig. 6). Before t = 2 s, the system operates in steady state with voltage balance control. The grid-side injected real and reactive power (P_s, Q_s) are 1 MW and 0 MVA. Input voltage is balanced for the MFT-based converter with V_{C1} = V_{C2} = V_{C3} = V_{C4} = V_{C5} = 1000 V. At t = 2 s, the voltage balance control scheme is deactivated (all five modules operate under the common duty cycle d_{common} [Fig. 6]). Although dc-link current (I_{dc}) and the real/reactive power are still being controlled effectively, the input capacitor voltages (V_{C1}, V_{C2}, V_{C3}, V_{C4}, and V_{C5}) begin to diverge. This reveals that voltage balance control of the modular converter is decoupled from other control objectives of the WECS (MPPT, dc-link current and reactive power control). V_{C1} is the highest (1180 V) because the duty ratio of its transformer (Module 1) is the lowest (Table I). At t = 2.5 s, the voltage balance control scheme is reactivated and input capacitor voltages quickly converge to nominal values.

Fig. 10 illustrates the simulated performance under stepped wind speed. To simulate the transient response of the WECS, wind speed is purposely set to step down and up from 12 m/s (1 pu) to 10 m/s (0.833 pu) at t = 2 s and from 10 m/s (0.833 pu) to 12 m/s (1 pu) at t = 4 s, respectively. The resultant reference speed w_{g_ref} changes accordingly (Fig. 10 (a)). The real speed w_g of the PMSG tracks the reference speed w_{g_ref} well in both steady and transient states. Real power P_s is the cube of generator speed w_g; therefore, only 0.57 pu of real power is captured (Fig. 10 [b]) when the wind speed is reduced to 0.833 pu. To minimize loss, a minimum dc-link current is altered accordingly (Fig. 10 [c]). The input capacitor voltages (V_{C1}, V_{C2}, V_{C3}, V_{C4}, and V_{C5}) are well balanced in all steady and transient states, as shown in Fig. 10 (d). Voltage spikes happen on the input capacitor during transient states. This is because (a) an overshoot happens for speed regulation (Fig. 10 [a]); (b) the input capacitor voltage of the converter is proportional to the induced voltage of the PMSG, which is in turn proportional to its speed w_g.

Fig. 11 presents the simulated performance under reactive power control. Reactive power Q_s is injected into the grid according to grid codes [3] with 330 kVA (0.33 pu) between 2 and 3 s, –330 kVA (–0.33 pu) between 4 and 5 s, respectively (Fig. 11 [a]). As in Fig. 10 (c), a minimum dc-link current is modified accordingly to minimize minimum loss (Fig. 11 [b]). Fig. 11 (c) shows that all input capacitor voltages are evenly distributed. The power factors (PF) for different reactive power levels (0, 0.33, –0.33 pu) are 1, 0.95, and –0.95, respectively, as per Fig. 12. V_A and i_{gA} are the grid-side phase voltage and the injected current, respectively.

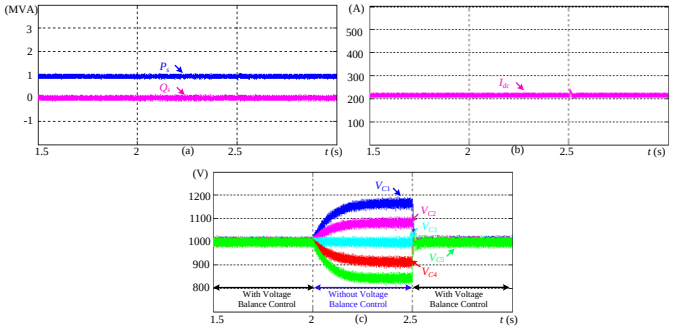

Fig. 9. Simulated performance of the proposed WECS under conditions of with/without voltage balance control. (a) Grid-side injected real and reactive power (P_s, Q_s); (b) Dc-link current I_{dc}; (c) Input capacitor voltages of the MFT-based cascaded dc-dc converter (V_{C1}, V_{C2}, V_{C3}, V_{C4}, and V_{C5}).

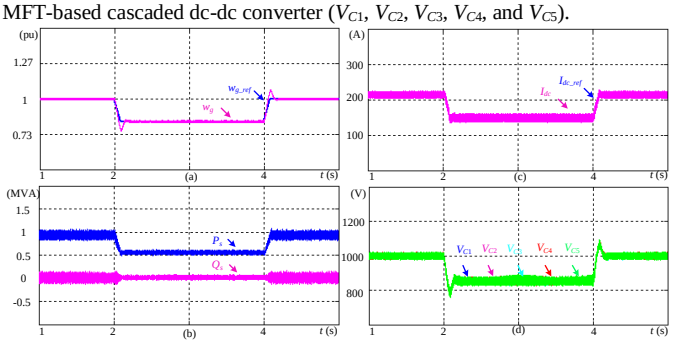

Fig. 10. Simulated performance of the proposed WECS under stepped wind speed. (a) Reference and real speed of the PMSG (w_{g_ref}, w_g); (b) Grid-side injected real and reactive power (P_s, Q_s); (c) Dc-link current (I_{dc}, I_{dc_ref}); (d) Input capacitor voltages of the MFT-based cascaded dc-dc converter (V_{C1}, V_{C2}, V_{C3}, V_{C4}, and V_{C5}).

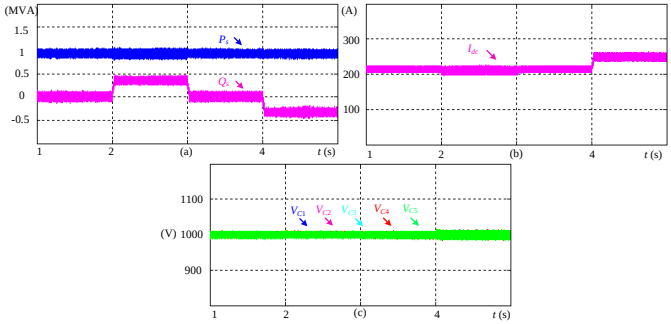

Fig. 11. Simulated performance of the proposed WECS under reactive power control. (a) Grid-side injected real and reactive power (P_s, Q_s); (c) Dc-link current (I_{dc}, I_{dc_ref}); (d) Input capacitor voltages of the MFT-based cascaded dc-dc converter (V_{C1}, V_{C2}, V_{C3}, V_{C4}, and V_{C5}).

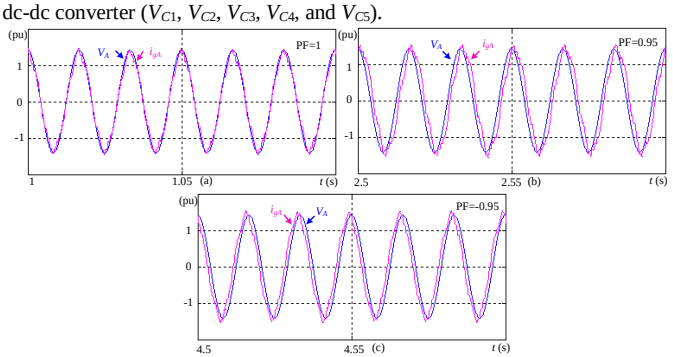

Fig. 12. Simulated waveforms of grid line voltage V_A and injected line current i_{gA}. (a) PF = 1(Q_s = 0 pu); (b) PF = 0.95(Q_s = 0.33 pu); (c) PF = – 0.95(Q_s = – 0.33 pu).

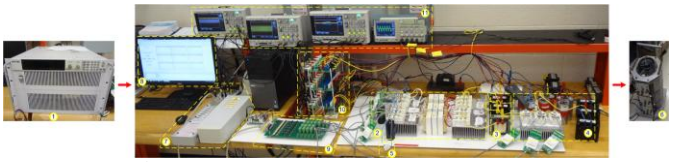

Fig. 13. Photo of the experimental setup. (1) Dc power supply. (2) MFT-based cascaded dc-dc converter. (3) Dc-link inductor. (4) Current source inverter. (5) Parallel resistor for imbalance. (6) Three-phase variac. (7) dSPACE DS1103 processor board. (8) dSPACE control desk on computer. (9) Driver interface board. (10) Voltage/current sensor boards. (11) Oscilloscope.

B. Experimental Results

The experimental setup is illustrated in Fig. 13. First, we simplify this setup by replacing the wind turbine–PMSG–diode rectifier by a dc voltage supply as the emphasis of this work is on verifying the performance of the proposed converter. Three MFT-based modules are employed as the front-end converter, and the turn ratios of the three MFTs are set to 1:1 (with a tolerance of ± 2%, as presented in Table I) to lower cost; a 400 ohm resistor is paralleled with the input capacitor of Module 3 on purpose to introduce imbalance into the modular converter; IGBT modules (SKM300GB12T4) and rectifier diodes (SKKD212) are used to construct this converter. The CSI is composed of three integrated modules (SKM300GBD12T4). A three-phase variac is also employed here with an input that connects the local grid and an output that connects CSI through a three-phase LC filter. dSPACE DS1103 is used to implement the control algorithms (Fig. 6) and to communicate with the dSPACE control desk of the computer. The inputs variables are sampled with transducers (LEM LA 100-P, LV 25-P) while the outputs are driver signals sent to drivers through an interface board. Finally four oscilloscopes are used simultaneously to capture the required waveforms. The modulation schemes are the phase-shifted PWM for the modular converter and the SVM for CSI. Same with simulation, three tests are performed to verify the performance of the proposed WECS.

Fig. 14 shows the experimental performance with/without the voltage balance control. V_{in} is the total input voltage; V_{C1} V_{C2}, and V_{C3} are the input capacitor voltage for Module 1, 2, and 3; I_{dc} is the measured dc-link current; and P_s and Q_s are the plotted real and reactive power based on measured voltages and currents, respectively. With voltage balance control, the converter operates well. Input voltages are balanced with V_{C1} = V_{C2} = V_{C3} = 83 V; the dc-link current is controlled at 8.5 A; and the grid-side injected real and reactive power (P_s, Q_s) are 1,275 W and 0 VA. As depicted in Fig. 14 (a), when the voltage balance control is deactivated (all the three modules operate under common duty cycle d_{common} [Fig. 6]), the input capacitor voltages (V_{C1}, V_{C2}, and V_{C3}) start diverging. V_{C3} decreases to the lowest voltage due to its paralleled resistor (400 ohm); V_{C1} and V_{C2} are unequal because of the turn-ratio tolerance of their transformers (± 2% as shown in Table I). DC-link current (I_{dc}) and the real/reactive power (P_s, Q_s) control, on the other hand, are not influenced. Again, this verifies that voltage balance control of the modular converter is decoupled from other control objectives (dc-link current and reactive power control). Subsequently, input capacitor voltages of the modular converter quickly converge to nominal values when the voltage balance control is reactivated. Fig. 15 illustrates the experimental performance under stepped input voltage (stepped wind speed in simulation) from 0.8 pu (200 V) to 1 pu (250 V). The dc-link current I_{dc} increases from 7.5 A to 8.5 A; moreover, injected real power P_s increases from approximately 0.52 pu (660 W) to 1 pu (1275 W) while the reactive power Q_s is maintained at zero. During all the steady and transient states, input capacitor voltages (V_{C1}, V_{C2}, and V_{C3}) are well balanced, as shown in Fig. 15 (a). In this figure, the waveforms for V_{C1}, V_{C2}, and V_{C3} are overlapped. Fig. 16 illustrates the experimental performance under reactive power control. Different reactive power Q_s (0, 0.33, –0.33 pu) are separately injected into the local grid (Fig. 16 [c]). Similarly, the minimum dc-link current I_{dc} is changed accordingly to minimize loss (Fig. 16 [b]). Input capacitor voltages V_{C1}, V_{C2}, and V_{C3} (Fig. 16 [a]) are distributed evenly during steady and transient states. Fig. 17 exhibits the steady-state, local grid line-to-line voltage V_{AB} (208 V) and the injected line current i_{gA} under different reactive powers. Fig. 17 (a) shows i_{gA} lags behind V_{AB} by around 30°; thus suggesting that a UPF is achieved. Similarly, i_{gA} lags behind V_{AB} by roughly 58° (Q_s = 0.33 pu, PF = 0.95) and 12° (P_s = –0.33 pu, PF = –0.95), as displayed in Fig. 17 (b) and Fig. 17 (c).

The performance of the injected line current i_{gA} (Fig. 17) is not as good as that in the simulation (Fig. 12). However, this is reasonable given this experimental setup. In contrast to VSC, where a period of dead time (about 1–2 µs) must be allocated for drive signals to avoid short-circuit operation, an overlap time is required for CSI to avoid open-circuit operation [17]. The performance of the outputs is substantially influenced by the dead/overlap time [35]; in this work, the overlap time for CSI switching devices is controlled by dSPACE DS1103. The minimum fixed step achieved is 50 µs when all the control schemes are processed (Fig. 6); therefore, the minimum overlap time for CSI is roughly 50 µs which is too large. Hence, the performance of the grid-connected current is poorer than that in simulation where the overlap time is 5 µs. Such a conclusion can be verified by Fig. 18 where the simulation is conducted under same overlap time as that in the experiment (50 µs). Nonetheless, this is no longer an issue in practice as processing frequency of the DSP/FPGA is at least 150 MHz (6.7 ns).

VI. CONCLUSION

In this work, an MFT-based WECS is proposed for CSC-based offshore wind farms. The proposed configuration is composed of an MV PMSG, a passive rectifier, a modular MFT-based converter, and a CSI. It is characterized by (a) no offshore substation; (b) high power density due to the adaption of a modular MFTs instead of a low-frequency transformer; (c) high reliability and flexibility due to the use of a modular converter; and (e) all the advantages of a CSC. Apart from traditional control objectives (MPPT, dc-link current and reactive power control) of a WECS, additional effort is made to ensure an evenly distributed power and voltage sharing among the constituent modules. The characteristic of decoupling between voltage/power balance control and the other control objectives is analyzed as well. Finally simulation and experimental verification are provided to demonstrate the converter's performance of the proposed WECS.

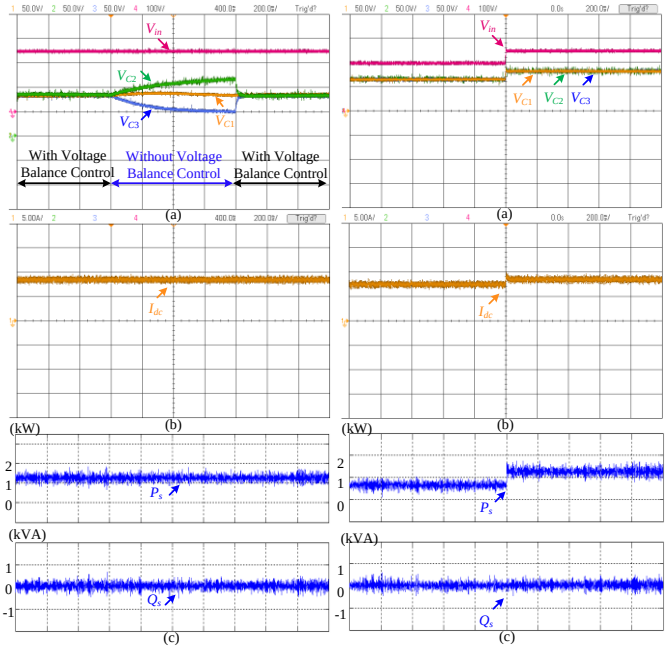

Fig. 14 (Left). Experimental converter's performance of the proposed WECS under condition of with/without voltage balance control.

Fig. 15 (Right). Experimental converter's performance of the proposed WECS under stepped input voltage. (a) Input capacitor voltages of the MFT-based cascaded dc-dc converter (V_{C1}, V_{C2}, and V_{C3}); (b) Dc-link current (I_{dc}); (c) Grid-side injected real and reactive power (P_s, Q_s).

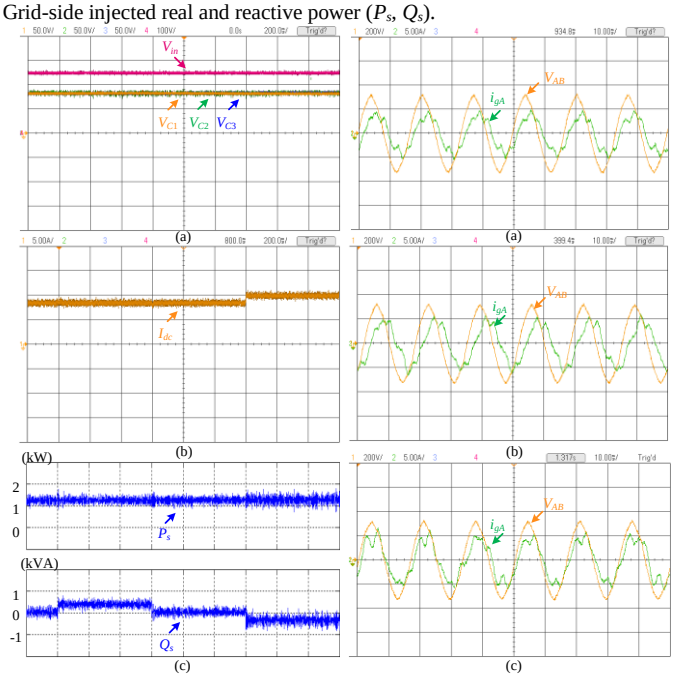

Fig. 16 (Left). Experimental converter`s performance of the proposed WECS under reactive power control. (a) Input capacitor voltages of the MFT-based cascaded dc-dc converter (V_{C1}, V_{C2}, and V_{C3}); (b) Dc-link current (I_{dc}); (c) Grid-side injected real and reactive power (P_s, Q_s).

Fig. 17 (Right). Experimental waveforms of grid line-to-line voltage (V_{AB}) and injected line current (i_{gA}). (a) PF = 1; (b) PF = 0.9; (c) PF = – 0.95.

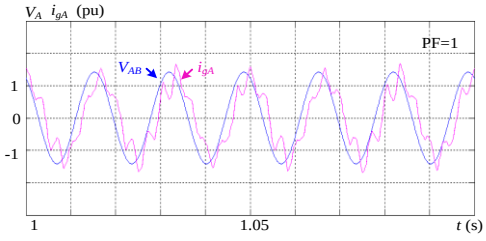

Fig. 18. Simulated waveforms of grid line-to-line voltage (V_{AB}) and injected line current (i_{gA}) under same overlap time as that in the experiment (50μs).

REFERENCES

[1] Global Wind Energy Outlook 2010, Global Wind Energy Council, London, U.K., 2010.

[2] The European Wind Energy Association (EWEA), Offshore Wind, 2014, accessed on Aug. 2014. [Online]. Available: http://www.ewea.org.

[3] B. Wu, Y. Lang, N. Zargari and S. Kouro, Power Conversion and Control of Wind Energy Systems. Wiley-IEEE Press, 2011.

[4] P. Bresesti, W. Kling, R. Hendriks, and R. Vailati, ''HVDC connection of offshore wind farms to the transmission system,'' IEEE Trans. Energy Convers., vol. 22, no. 1, pp. 37–43, Mar. 2007.

[5] N. Flourentzou, V. Agelidis, andG. Demetriades, ''VSC-based HVDC power transmission systems: An overview,'' IEEE Trans. Power Electron., vol. 24, no. 3, pp. 592–602, Mar. 2009.

[6] C. Meyer, M. Hoing, A. Peterson, and R. De Doncker, ''Control and design of DC grids for offshore wind farms,'' IEEE Trans. Ind. Appl., vol. 43, no. 6, pp. 1475–1482, Nov. 2007.

[7] E. Veilleux and P. Lehn, ''Interconnection of direct-drive wind turbines using a series-connected DC grid,'' IEEE Trans. Sustain. Energy, vol. 5, no. 1, pp. 139–147, Jan. 2014.

[8] Venkata Yaramasu, Bin Wu, Paresh C. Sen., "High-Power Wind Energy Conversion Systems State-of-the-Art and Emerging Technologies," Proceedings of IEEE. DOI: 10.1109/JPROC.2014.2378692.

[9] Z. Zhu and J. Hu, ''Electrical machines and power-electronic systems for high-power wind energy generation applications: Part IIVPower electronics and control systems,'' COMPEL: Int. J. Computat. Math. Elect. Electron. Eng., vol. 32, no. 1, pp. 34–71, 2013.

[10] E. Bueno, S. Cobreces, F. Rodriguez, A. Hernandez, and F. Espinosa, ''Design of a back-to-back NPC converter interface for wind turbines with squirrel-cage induction generator,'' IEEE Trans. Energy Convers., vol. 23, no. 3, pp. 932–945, Sep. 2008.

[11] A. Faulstich, J. Stinke, and F. Wittwer,''Medium voltage converter for permanent magnet wind power generators up to 5 MW,'' in Proc. Eur. Conf. Power Electron. Appl. (EPE), Dresden, Germany, 2005, p. 9-P.9.

[12] S. Kouro et al., ''Recent advances and industrial applications of multilevel converters,'' IEEE Trans. Ind. Electron., vol. 57, no. 8, pp. 2553–2580, Aug. 2010.

[13] V. Yaramasu and B. Wu, ''Model predictive decoupled active and reactive power control for high-power grid-connected four-level diode-clamped inverters,'' IEEE Trans. Ind. Electron., vol. 61, no. 7, pp. 3407–3416, Jul. 2014.

[14] J. Li, S. Bhattacharya, and A. Huang, ''A new nine-level active NPC (ANPC) converter for grid connection of large wind turbines for distributed generation,'' IEEE Trans. Power Electron., vol. 26, no. 3, pp. 961–972, Mar. 2011.

[15] A. Zuckerberger, D. Weinstock, and A. Alexandrovitz, ''Single-phase matrix converter,'' IEE Proc. Electr. Power Appl., vol. 144, no. 4, pp. 235–240, Jul. 1997.

[16] J. Wang, D. Xu, B. Wu, and Z. Luo, ''A low-cost rectifier topology for variable-speed high-power PMSG wind turbines,'' IEEE Trans. Power Electron., vol. 26, no. 8, pp. 2192–2200, Aug. 2011.

[17] B. Wu, High-Power Converters and AC Drives. New York/Piscataway, NJ: Wiley/IEEE Press, 2006.

[18] Z. Chen, "Compensation schemes for a SCR converter in variable speed wind power systems," IEEE Trans. Power Del., vol. 19, no. 2, pp. 813–821, Apr. 2004.

[19] P. Tenca, A. A. Rockhill, T. A. Lipo, and P. Tricoli, "Current source topology for wind turbines with decreased mains current harmonics, further reducible via functional minimization," IEEE Trans. Power Electron., vol. 23, no. 3, pp. 1143–1155, May 2008.

[20] S. Nishikata and F. Tatsuta, "A new interconnecting method for wind turbine/generators in a wind farm and basic performances of the integrated system," IEEE Trans. Ind. Electron., vol. 57, no. 2, pp. 468–475, Feb. 2010.

[21] J. M. Carrasco et al., "Power-electronic systems for the grid integration of renewable energy sources: A survey," IEEE Trans. Ind. Electron., vol. 53, no. 4, pp. 1002–1016, Jun. 2006.

[22] Yuanye Xia; Ahmed, K.H.; Williams, B.W. "A PWM Current Source-Based DC Transmission System for Multiple Wind Turbine

Interfacing", Emerging and Selected Topics in Power Electronics, IEEE Journal of, On page(s): 784 - 796 Volume: 2, Issue: 4, Dec. 2014

[23] J. Dai, D. Xu, and B. Wu, "A novel control scheme for current-source converter- based PMSG wind energy conversion systems," IEEE Trans. Power Electron., vol. 24, no. 4, pp. 963–972, Apr. 2009.

[24] M. Popat, B.Wu, F.Liu and N. Zargari, "Coordinated control of cascaded current source converter based offshore wind farms," IEEE Trans. on Sustainable Energy, vol. 3, no. 3, pp. 557-565, 2012.

[25] Blaabjerg, F.; Ke Ma "Future on Power Electronics for Wind Turbine Systems", Emerging and Selected Topics in Power Electronics, IEEE Journal of, on page(s): 139 - 152 Volume: 1, Issue: 3, Sept. 2013.

[26] Y. Xia, J. Fletcher, S. Finney, K. Ahmed, and B. Williams, "Torque ripple analysis and reduction for wind energy conversion systems using uncontrolled rectifier and boost converter," IET Renew. Power Gener., vol. 5, no. 5, pp. 377–386, Sep. 2011.

[27] X. Tan, J. Dai and B. Wu "A novel converter configuration for wind applications using PWM CSI with diode rectifier and buck converter", *Proc. IEEE Int. Electr. Mach. Drives Conf.*, pp.359 -364.

[28] J.W. Kolar, G. Ortiz, Solid-State Transformers, Plenary Session Presentation at the IEEE International Power Electronics and Applications Conference and Exhibition (PEAC 2014), Shanghai, Nov. 5-8, 2014.

[29] J.A.Sabate, V.Vlatkovic, R.B.Ridley, F.C.Lee, and B.H.Cho, "Design considerations for high voltage high power full bridge zero voltage switched PWM converter", IEEE APEC'90, p275-284.

[30] G. Ortiz, J. Biela and J. W. Kolar "Optimized design of medium frequency transformers with high isolation requirements", Proc. 36th IEEE IECON/IECON, pp.631 -638 2010.

[31] R. Giri, V. Choudhary, R. Ayyanar, and N. Mohan, "Common-duty ratio control of input-series connected modular dc-dc converters with active input voltage and load-current sharing," *IEEE Trans. Ind. Appl.*, vol. 42, no. 4, pp. 1101–1111, Jul./Aug. 2006.

[32] Dai, Jingya, "Current source converters for megawatt wind energy conversion systems" (2010). Theses and dissertations. Paper 841.

[33] M. Popat , B. Wu and N. Zargari "A novel decoupled interconnecting method for current-source converter-based offshore wind farm", IEEE Trans. Power Electron., vol. 27, no. 10, pp.4224 -4233 2012.

[34] Qiang Wei; Bin Wu. "Analysis and comparison of current-source-converter-based medium-voltage PMSG wind energy conversion systems", Power Electronics for Distributed Generation Systems (PEDG), 2015 IEEE 6th International Symposium on, On page(s): 1 - 6

[35] L. Chen and F. Z. Peng, "Dead-time elimination for voltage source inverters," IEEE Trans. Power Electron., vol. 23, no. 2, pp. 574–580, Mar. 2008.

[36] M. Guan and Z. Xu, "A novel concept of offshore wind-power collection and transmission system based on cascaded converter topology", International Transactions on Electrical Energy Systems. vol. 24, no. 3, pp. 363-377, 2014.

[37] D. Jovcic, "Offshore wind farm with a series multiterminal CSI HVDC," Electr. Power Syst. Res., vol. 78, no. 4, pp. 747–755, Apr. 2008.

[38] E. Agheb and H. Hoidalen, "Medium frequency high power transformers, state of art and challenges," in Renewable Energy Research and Applications (ICRERA), 2012 International Conference on, 2012, pp. 1–6.

Qiang Wei received the B.sc degree from Henan University of Science and Technology, Luoyang, China, in 2008, and the M.A.Sc degree from Xi'an Jiaotong University, Xi'an, China, in 2012 both in electrical engineering, where he is currently working toward the Ph.D. degree in electrical engineering at Ryerson University, Toronto, ON, Canada. From 2012 to 2014, he was with the Delta Power Electronics, Nanjing, China, as an R&D Engineer. His research interests include electric motor drives, power converter systems, and renewable energy systems.

Bin Wu (IEEE S'89–M'92–SM'99-F'08) received his M.A.Sc. and Ph.D. degrees in electrical and computer engineering from the University of Toronto, Canada in 1989 and 1993, respectively. He joined Ryerson University in 1993, where he is currently a Professor and Senior NSERC/Rockwell Automation Industrial Research Chair in Power Electronics and Electric Drives. Dr. Wu has published more than 350 technical papers, authored/coauthored two Wiley-IEEE Press books, and holds more than 30 granted/pending US/European patents in the area of power conversion, medium voltage drives, and renewable energy systems. Dr. Wu received the Gold Medal of the Governor General of Canada in 1993, Premier's Research Excellence Award in 2001, NSERC Synergy Award for Innovation in 2002, Ryerson Distinguished Scholar Award in 2003, Ryerson YSGS Outstanding Contribution to Graduate Education Award and Professional Engineers Ontario (PEO) Engineering Excellence Medal in 2014. He is a fellow of Engineering Institute of Canada (EIC) and Canadian Academy of Engineering (CAE).

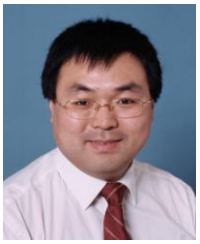

Dewei (David) Xu (S'99–M'01) received the B.Sc, M.A.Sc, and Ph.D. degrees in electrical engineering from Tsinghua University, Beijing, China, respectively in 1996, 1998, and 2001. He has been working in Ryerson University, Toronto, Ontario since 2001, where he is currently Professor. His research interests include renewable energy system, high power converters, electric motor drives and advanced digital control for power electronics.

Navid R. Zargari (IEEE M'94–SM'08–F'15) received the B.Eng. degree from Tehran University, Iran, in 1987 and the M.A.Sc. and Ph.D. degrees from Concordia University, Montreal, Quebec, Canada, in 1991 and 1995 respectively. He has been with Rockwell Automation Canada since November 1994, first as a senior designer, then as the manager of the Medium Voltage R&D department and currently as a Product Architect. For the past 19 years he has been involved with simulation, analysis and design of power converters for Medium Voltage AC drives. His research interests include power converter topologies and their control aspects, power semiconductors and renewable energy sources. Dr. Zargari has co-authored more than 80 research papers as well as a book on Power Conversion and Control of Wind Energy Systems. He holds 30 US granted/pending patents in power converters and Medium Voltage applications and was the recipient of the Premier's Award for the Innovator of the year in 2009 from the Province of Ontario.